HHS Public Access

Author manuscript

Hear Res. Author manuscript; available in PMC 2021 May 01.

Published in final edited form as:

Hear Res. 2020 May ; 390: 107935. doi:10.1016/j.heares.2020.107935.

Pericyte Abnormalities Precede Strial Capillary Basement Membrane Thickening in Alport Mice

Brianna Dufek[*], **Daniel T. Meehan**[*], **Duane Delimont**[*], **Gina Samuelson**[*], **Jacob Madison**[*], **Xiourui Shi**[+], **Flint Boettcher**[#], **Michael Anne Gratton**[#], **Vincent Trosky**[#], **Dominic Cosgrove**[*]

[*]Boys Town National Research Hospital, Omaha, NE

[+]Oregon Health and Science Center, Portland, OR

[#]Washington University, Saint Louis MO

Abstract

In 129 Sv autosomal Alport mice, the strial capillary basement membranes (SCBMs) progressively thicken between 5 and 9 weeks of age resulting in a hypoxic microenvironment with metabolic stress and induction of pro-inflammatory cytokines and chemokines. These events occur concomitant with a drop in endocochlear potential and a susceptibility to noise-induced hearing loss under conditions that do not permanently affect age/strain-matched littermates. Here we aimed to gain an understanding of events that occur before the onset of SCBM thickening. Alport stria has normal thickness and shows levels of extracellular matrix (ECM) molecules in the SCBMs commensurate with wild-type mice. Hearing thresholds in the 3-week Alport mice do not differ from those of wild-type mice. We performed RNAseq analysis using RNA from stria vascularis isolated from 3-week Alport mice and wild type littermates. Data was processed using Ingenuity Pathway Analysis software and further distilled using manual procedures. RNAseq analysis revealed significant dysregulation of genes involved in cell adhesion, cell migration, formation of protrusions, and both actin and tubulin cytoskeletal dynamics. Overall, the data suggested changes in the cellular architecture of the stria might be apparent. To test this notion, we performed dual immunofluorescence analysis on whole mounts of the stria vascularis from these same animals stained with anti-isolectin gs-ib4 (endothelial cell marker) and anti-desmin (pericyte marker) antibodies. The results showed evidence of pericyte detachment and migration as well as the formation of membrane ruffling on pericytes in z-stacked confocal images from Alport mice compared to wild type littermates. This was confirmed by TEM analysis. Earlier work from our lab showed that endothelin A receptor blockade prevents SCBM thickening and ECM accumulation in the SCBMs. Treating cultured pericytes with endothelin-1 induced actin cytoskeletal rearrangement, increasing the ratio of filamentous to globular actin. Collectively, these findings suggest that the change in type IV collagen composition in the Alport SCBMs

Corresponding Author: Dominic Cosgrove, Ph.D., Director, Center for Sensory Neuroscience, Boys Town National Research Hospital, 555 North 30th St., Omaha NE 68131, Phone: 531-355-6334, Dominic.cosgrove@boystown.org.

Author Statement: The authors of this work have no conflicts of interest to disclose.

results in cellular insult to the pericyte compartment, activating detachment and altered cytoskeletal dynamics. These events precede SCBM thickening and hearing loss in Alport mice, and thus constitute the earliest event so far recognized in Alport strial pathology.

Keywords

Strial capillary basement membrane; Alport syndrome; RNA-seq; pericyte

Introduction

Alport syndrome is a basement membrane collagen disorder characterized by glomerular dysfunction associated with delayed onset and progressive hearing loss. Genetically, it is associated with mutations in the basement membrane collagen α3 (IV), α4(IV) or α5(IV) genes (Barker et al., 1990; Mochizuki et al., 1994). In the renal glomerulus, absence of this collagen network results in progressive breakdown of the glomerular basement membrane resulting in podocyte injury and renal failure. In the inner ear of a gene knockout mouse model (a collagen α3(IV) mutant) the strial capillary basement membranes (SCBMs) become progressively thickened, resulting in a hypoxic microenvironment that is associated with susceptibility to moderate-noise induced hearing loss (Cosgrove et al., 1998; Gratton et al., 2005; Meehan et al., 2016). The thickening of the SCBMs is associated with elevated levels of extracellular matrix molecules including laminin 211, laminin 521, entactin, and type IV collagen α1/α2 networks (Gratton et al., 2005; Meehan et al., 2016).

In earlier work we demonstrated that the stria vascularis in 7-week-old Alport mice, an age where the SCBMs are significantly thickened, shows signs of metabolic and oxidative stress, with significant up-regulation of VEGF, Hif1-α, and Glut1. (Cosgrove et al., 1998; Meehan et al., 2016). This was associated with accumulation of extracellular matrix molecules in the SCBM including type IV collagen, laminin 211, and laminin 521. Given that Alport strial dysfunction is delayed onset and progressive, we performed RNA-seq analysis on 3-week-old Alport mice, an age where the SCBMs are not significantly thickened and when there is no hearing loss in order to gain an understanding of the early events in Alport strial pathogenesis. We noted fewer than 40 genes were significantly dysregulated. They fell primarily into categories of cell adhesion, formation of cell protrusions, regulation of small GTPases, and regulation of actin and tubulin cytoskeletal components. Collectively this suggested that cellular dysmorphology in the 3-week stria may be apparent. Whole mount immunofluorescence analysis revealed pericyte protrusions, detachment, and migration, suggesting abnormalities in the pericyte compartment. These findings were confirmed by transmission electron microscopy (TEM). Cultured pericytes responded to endothein-1 treatment by increasing the ratio of filamentous actin to glomerular actin, suggesting that previously documented elevated levels of endothelin-1 in the Alport stria (Meehan et al., 2016) is activating changes in actin cytoskeletal dynamics in the pericyte compartment. This is the earliest pathologic event identified in the Alport stria and very similar to what we previously reported in the renal glomerulus of Alport mice (Dufek et al., 2016).

Methods

Mice

129 Sv autosomal Alport mice were developed in the Cosgrove lab (Cosgrove et al., 1996). All mice were on a pure 129 Sv genetic background and maintained in house. All procedures involving animals were conducted in accordance of an approved IACUC protocols at both sites (Boys Town National Research Hospital and Washington University) and consistent with the NIH guide for the care and use of laboratory animals. Every effort was made to minimize usage as well as minimize any pain or distress. Both males and females were utilized. Animals were housed in groups with in rooms with a 14/10 hour light/dark cycle (BTNRH) or 12/12/ hour light/dark cycle (WU).

Morphometric measures of SCBM width

SCBMs from at least 5 cochleae each from 3-week-old wild type and Alport mice were examined by transmission electron microscopy for SCBM width. 3 different mid-modiolar cross-sections were processed for each ear. All strial capillaries were measured along at least 10 points per capillary.

Strial microdissection

A detailed procedure for strial microdissection was described previously (Gratton et al., 2005). The temporal bones were harvested from non-perfused mice following cervical dislocation (within two minutes) and transferred to ice-cold HBSS buffer in a specialized petri dish. Both stria were microdissected within 10 minutes and transferred to TriZol for later RNA isolation. The stria from nine wild type and nine Alport mice were collected and the RNA from 3 individual mice combined for a single analysis which was performed three independent times.

Auditory brainstem response

ABR measures were performed as previously described (Meehan et al., 2016).

RNA-seq analysis

Microdissected striae were lysed in Trizol® (Ambion®, Carlsbad, CA) and RNA isolated from the aqueous phase using PureLink® RNA Mini Kit (Ambion®). An RNA Quality Number (RQN) was determined for each sample using a Fragment Analyzer™ Automated CE System (Advanced Analytical Technologies, Inc. Ames, IA). Samples with RQN's of ≥ 8 were used in SMART-Seq®v4 Ultra® (Takara Bio USA, Inc.). cDNA synthesis and libraries generated utilizing Nextera™ XT DNA Library Preparation Kit (Illumina® San Diego, CA). RNA seq analysis was performed using Illumina® NextSeq™ 550 system (San Diego, CA). Ten ng input of Strial RNA was used for cDNA/library generation. The data was analyzed using Ingenuity Pathway Analysis software (QIAGEN Bioinformatics) by the University of Nebraska Medical Center bioinformatics core facility. This is a somewhat generic classification of the data into categories and then sub-categories. For example, major categories include canonical pathways, transcriptional regulators, disease functions, and toxicity functions. These are further broken down to sub-categories; for example the major

category of disease functions breaks down to sub-categories of immunological disease, metabolic disease endocrine disorders and organismal injury. For each subcategory the molecules that are significantly modulated and the degree of that modulation are listed. Given that the program was written as for broad-spectrum analysis, we further distilled our data manually into the data presented in Table 1. Standard deviations are provided for three independent RNA-seq experiments.

Generation of Heat map

TPM (transcripts per million) values from Ingenuity Pathway Analysis (QIAGEN) were trimmed of pseudogenes, predicted genes, and RIKEN cDNA clones; then normalized using a mean of means approach with ATP5F1, PGK1, and GAPDH used for normalization (Panina et al. 2018). A target value for all samples and sets of housekeeping genes X was utilized with other samples to produce a scaling factor Y for each sample (example S1), which was then applied to every TPM value within the original Ingenuity dataset.

$$X = \frac{\sum \frac{TPM_{HK1} + TPM_{HK2\cdots}}{n_{HK}}}{n_{samples}}$$

$$Y_{S1} = \frac{X}{\left(\frac{TPM_{HK1_{S1}} + TPM_{HK2_{S1}\cdots}}{n_{HK}}\right)}$$

$$TPM_{norm_{S1}} = TPM_{original} \cdot Y_{S1}$$

Using the Gene Set Enrichment Analysis version 4.0.3 software from the Broad Institute, the Curated 3wk Stria TPM Values from 3wk Alport and Wild Type samples were analyzed to the c5.all.v7.0.symbols gene dataset from the Molecular Signatures Database v7.0 by the Broad Institute. This dataset includes all gene sets annotated by the Gene Ontology Consortium. GSEA was run at 10,000 permutations, 3wk Alport vs. 3wk Wild Type Stria Vascularis, maximum gene set size of 750, and minimum of 5. The overall differentially expressed genes heatmap is shown in Figure 4. GSEA ranked gene set outputs for both Alport and Wild Type phenotypes are in supplementary information. The ranked gene list is included which denotes the highest scored differentially expressed genes according to the GSEA algorithm (Subramanian et al. 2005). Raw TPM Values are in an excel spreadsheet (supplementary data). The heatmap/gene set data for the statistically significant differentially expressed gene set, at the level of $p < .05$, false discovery rate (FDR) < 25%, and Family wise error rate (FWER) <5%.

Immunofluorescence analysis

Cochleae were perfused with 4% paraformaldehyde and then decalcified overnight in 150mM EDTA on a rotator at 4°C. The samples were transferred to 15% sucrose for 1 hour

and then into 30% sucrose for 2 hours. Samples were mounted in OCT and frozen at −80°C. Cochleae were sectioned at 8-μm and dipped in cold acetone. After air-drying 2 hours, slides were rehydrated with 1X PBS. Cochleae sections used for collagen IV immunostaining were first denatured with acid urea (6M urea, 0.1M glycine, pH 3.5) for 1 hour at 4°C and then rinsed with 1X PBS. Slides were stained with one of the following antibodies: rat anti-mouse Laminin α2 antibody (L0663, Sigma-Aldrich, St. Louis, MO, USA) at 1:500, rabbit anti-mouse Laminin α5 antibody (a gift from Jeff Miner, Washington University) at 1:1500, rabbit anti-mouse Collagen α1IV antibody (T40261R, Biodesign, Saco, ME, USA) at 1:500. Sections were incubated overnight at 4°C in a humidified chamber with their primary antibodies diluted in 0.1% PBST (Triton X-100) + 5% FBS. Slides were rinsed with 1X PBS and incubated with the appropriate Alexa Fluor secondary antibodies at 1:500 for 1 hour at room temperature. The slides were rinsed again with 1X PBS and mounted with Vectashield Mounting Medium with Dapi (H-1200, Vector Laboratories, Burlingame, CA, USA).

Pericyte immunostaining

PCs were obtained from Dr Shi's lab at passage 8–9. The derivation and characterization of these cells was described in detail in Neng et al., (2013). PCs were grown and ET-1 treated (3.5 ug/ml for 30 minutes) on collagen type 1- coated cytology slides (VWR, Batavia, IL). Slides were rinsed with PBS, fixed with −20°C acetone for 5 minutes and dried for 2 hours at 25°C. Slides were rehydrated with PBS for 5 minutes, permeabilized with 0.1% Triton X-100 (Sigma, St. Louis, MO) in PBS for 5 minutes, followed by three successive PBS washes and then blocked with 2% FCS, 0.2% fish gelatin (Sigma) in PBS for 2 hours. The slides were incubated in blocking solution with 1:200 of an anti-Drebrin mouse monoclonal antibody (MAI-20377 Invitrogen Carlsbad, CA) overnight at 4°C. After three PBS washes, slides were incubated in blocking solution with a 1:500 dilution of Alexa Fluor 555 donkey anti-mouse IgG (A31570 Invitrogen) and 1:100 Alexa Flour 488 Phallodin (A123379 Molecular Probes Eugene, OR) for 2 hours. After three PBS washes, slides were cover-slipped ProLong™ Gold antifade reagent with DAPI (P36931 Invitrogen). Final images were assembled using Adobe Photoshop and Illustrator software (Adobe Systems San Jose, CA).

Whole mount strial immunostaining

Mice were perfused transcardially with PBS followed by 4% paraformaldehyde. Cochleae were dissected and fixed in paraformaldehyde overnight. Cochleae were washed in PBS for 15 minutes, the stria dissected, and mounted on slides pre-coated with Cell-Tak (Fisher) into a drop of PBS. The PBS is aspirated away to allow the stria to adhere to the slide, and then permeabilized using 0.5% Triton X-100 in 1X PBS for 30 minutes. A pre-block of 1% fish gelatin in PBS is applied for 1 hour, then primary antibodies added and incubated overnight in 1% BSA and 1X PBS. We used anti-desmin (1:50, abcam, cat#ab32362) and fluorescence-labeled isolectin GS-IB4 (1:300, Invitrogen, cat#121411, Alexa fluor 488), or anti-PDGFRb (1:100, Santa Cruz, Cat # sc-6252, Lot # G149). The secondary antibody for anti-desmin was anti-rabbit at 1:400 or for PDGFRb, anti-mouse at 1:400. The next day the slides were washed 3X for 10 minutes each with PBS and incubated with the secondary antibody for 1 hour at room temperature and mounted using Prolong gold mounting medium.

F-actin/G-actin Assay

To measure the ratio of F-actin to G-actin in primary strial pericyte cells (PCs) in response to ET-1 treatment, an F/G assay was performed. Cells were propagated to 80 % confluency in 5 % FCS-containing media on Rat tail type 1 collagen-coated dishes. The serum was subsequently reduced to 0.05% over the course of 7 days and the cells treated with 3.5μg/ml ET-1 free peptide. After 30 minutes of ET-1 treatment, the cells were lysed and processed as per manufacturer protocol (Cytoskeleton, CAT # BK037, Denver, CO). Cells were lysed and homogenized in detergent-based lysis buffer, centrifuged at low speed to remove debris and then centrifuged at high speed to differentially separate the G-actin (supernatant) from the F-actin (pellet). The pellets were lysed in a volume (equal to the supernatant ~700 μl) of 8M Urea. Aliquots of both fractions were mixed with 5 X SDS-loading buffer and immediately frozen at −20°C. 10 μl of each fraction was loaded and run on a 10% acrylamide gel and the protein transferred to PVDF membrane. The membrane was blocked in 5% milk in PBS with 0.1% Triton (PBST) for ≥ 1 hour and incubated overnight with a 1:2000 dilution of anti-pan actin, rabbit polyclonal antibody (Cytoskeleton, AAN01-A) in 0.1% Milk/PBST. The membrane was washed 4X for 5minutes with PBST at room temperature. A 1:20,000 dilution of goat anti-rabbit HRP antibody in 5% milk/PBST was then applied for ≥ 1 hour and washed as before. The membrane was developed using ECL Plus® for the detection of actin, exposed to film and Image J (NIH) used to quantify relative densities of the bands. The experiment was performed four separate times and produced consistent results.

Confocal Microscopy

Confocal images captured using a Leica TCS SP8 MP confocal imaging system, using a 63x NA: 1.4 oil or 10x NA: 0.3 objective. Final figures were assembled using Adobe Photoshop and Illustrator software.

Statistical analysis

For F/G actin ratios; the experiment was performed four separate times and analyzed by 2-tailed student's t test with significance set at $p< 0.05$. for RNA-seq studies three independent RNA-seq experiments were performed and analyzed by one-tailed student's t-test. For ABRs the experiment was performed on 5 individual animals per group and the data analyzed by 2-Way ANOVA, post-hoc Holm-Sidak. For RT-PCR analyses, the experiment was performed in triplicate and analyzed by two-tailed student's t-test.

Results

The cellular architecture of the stria vascularis is shown in cartoon form (left panel) and by TEM image (right panel) in Figure 1. We previously analyzed the strial RNA from 7-week-old Alport mice and wild type littermates by RT-PCR (Meehan et al., 2016). Several genes were shown to be dysregulated in the Alport stria. These include not only genes encoding ECM proteins known to accumulate in the SCBMs of Alport mice, but indicators of oxidative and metabolic stress including HIF-1α, VEGF, and Glut-1.

At 3 weeks of age, all the cochlear basement membranes are of comparable thickness to that of wild-type littermates, including the strial capillary basement membranes (56.9 ± 15.53 nm

for WT; 65.5 ± 12.49 nm for Alport). The 3-week-old Alport mice have normal hearing, as determined by auditory brainstem response (Figure 2). We previously reported that extracellular matrix accumulates in the SCBMs likely contributing to the observed SCBM thickening (Gratton et al., 2005; Meehan et al., 2016). Figure 3 shows elevated levels of ECM molecules in the SCBMs are not evident in the 3-week-old Alport mice relative to wild type littermates. Thus, like humans, hearing loss is delayed onset and progressive in the COL4A3 knockout mouse model for Alport syndrome.

To determine if early events in Alport strial pathogenesis might be present in the 3-week-old Alport mice, we performed RNAseq analysis using microdissected stria vascularis as the source of RNA. Stria from 9 mice from each genotype (3 week wild type and Alport) were pooled into 3 groups (3 animals per group) for analysis. The strial cDNA was analyzed using an Illumina^{R} NEXTSeq™ SSD system and the data analyzed using Ingenuity Pathway Analysis software (QIAGEN Bioinformatics). Data points represent the mean with standard deviation for the 3 groups. Data was analyzed as described in the methods and a heatmap generated (Figure 4). The heatmap shows the variability from individual sample to sample for the 3 RNA-seq runs as well as the reproducibility for up- and down-regulated genes. Dysregulated Genes that predicted a functional change in strial health are shown in Table 1. These genes fell into categories for their known regulation of cell adhesion, formation of protrusions, actin and tubulin cytoskeletal dynamics and the regulation of small GTPases. More specifically, for example, versican, which is up-regulated by 11-fold reduces adhesive interactions by blocking integrins (Wu et al., 2005), while catenin α2, which is down-regulated 2.5 fold, links adhesion receptors to the cytoskeleton (Drees et al., 2005). MICAL2, which is down regulated, promotes depolymerization of actin (Giridharan et al., 2012), while RP1, which is up-regulated 2.6-fold, regulates microtubule depolymerization (Liu et al., 2012). It is notable that there is no overlap with the RNA-seq data for the 7-week-old WT and Alport stria (Table 1), proving that these early events are mechanistically distinct from later events in the progression of Alport strial pathology. Collectively, the pattern of gene regulation suggested that cellular defects might exist in the stria of these mice at the adhesive interface with the SCBMs, presumably precipitated by the change in the basement membrane collagen composition.

To test this notion, dual labeling of whole mount stria vascularis preparations was performed using Alexa 488-labeled isolectin gs-ib4, which labels vascular endothelium, and anti-desmin, which labels pericytes (Figures 5). At 3 weeks of age we observe pericyte detachment associated with membrane ruffling (Figure 5B and D, asterisks), as well as migrating pericytes that have fully detached and are now in the interstitium of the stria (Figure 5B, arrowheads). At 7 weeks, both wild type and Alport stria vascularis appeared normal using these same methods (data not shown). Since desmin labels the pericyte filaments we did a second dual stain using PDGFRb, which stains the pericyte soma combined with desmin to visualize the pericyte filaments. The result in Figure 6B clearly shows a migrating pericyte (arrowhead) in the 3-week Alport whole mount stria where the soma is isolated, and the filaments radiate towards the strial vessels. We never observed this in the wild type whole mount stria (Figure 6A).

To further validate this phenomenon we conducted TEM analysis on stria capillaries from 3 week old wild type and Alport mice. The results in Figure 7A and C show tight adhesion of pericytes to the SCBMs at both the endothelial and epithelial contacts in the wild type stria. In the Alport stria we occasionally (approximately 1 in 10 capillaries examined) observed separation of pericytes from the SCBMs at both the epithelial and endothelial contacts (Figure 7B and D, arrowheads). These at times were severe with wide gaps forming (Figure 7D, arrow) and what appears to be membrane ruffling (Figure 7D asterisks).

In a recent report we showed that endothelin-1 (ET-1) activates actin cytoskeletal dynamics in glomerular mesangial cells (pericytes) in the kidney (Dufek et al., 2016). We also showed in earlier work that blocking the endothelin A receptor (ET_AR) prevented accumulation of extracellular matrix and thickening in the strial capillary basement membranes (Meehan et al., 2016). While it is clear that actin cytoskeletal dynamics are affected in the 3-week-old Alport stria vascularis, it is not clear whether ET-1 is inducing these effects as it does in the Alport glomerulus. We first examined RNA from isolated stria vascularis and cultured pericytes to see if they express ET_ARs. The results in Figure 8 show that indeed they do. To test this their response to ET-1, we cultured primary pericytes from 10–15 day old mice as described in Neng et al., (2013). Cells were treated with 3.5 μg/ml ET-1 for 30 minutes and assayed by western blot for the ratio of filamentous actin to globular actin. As shown in Figure 9A, F/G actin ratios are significantly higher in the treated cells compared to cells treated with a scrambled peptide (shown quantitatively in Figure 9B), thus proving ET-1-mediated activation of cytoskeletal rearrangements in strial pericytes. This observation was further confirmed by dual staining of the strial pericytes with phalloidin (green). Figure 10B shows that the treated cells show an abundance of actin stress fibers when compared the non-treated cells (Figure 10A), or cells pretreated with the small molecule inhibitor for ET_AR, Atrasentan (Figure 10C), before exposure to ET-1. This data is consistent with the biochemical analysis shown in Figure 9, where ET-1 treated cells show a greater abundance of filamentous actin.

Discussion

Alport syndrome presents with pathologies in both the renal glomerulus and the inner ear. It is therefore reasonable to consider that the pathologies might be somewhat related mechanistically. In earlier work we described a mechanism for disease initiation in Alport glomerular disease in which induction of ET-1 activates mesangial cells (glomerular pericytes) results in filopodial invasion of the sub-endothelial spaces of the glomerular capillaries (Zallocchi et al., 2013; Dufek et al., 2016). The filopodia deposit mesangial proteins in the GBM, of which laminin 211 activates focal adhesion kinase leading to a pro-inflammatory response in glomerular podocytes (Delimont et al., 2014). Investigating this mechanism in the cochlea of Alport mice, we noted laminin 211 protein was also markedly induced in the capillary basement membranes of the stria vascularis. As in the glomerulus, this was associated with focal adhesion kinase activation and activation of pro-inflammatory response mechanisms (Meehan et al., 2016). In both the cochlea and the renal glomerulus, matrix accumulation and basement membrane thickening could be prevented by blocking the endothelin A receptor (ET_AR) using the small molecule inhibitor Sitaxentan (Dufek et al 2016; Meehan et al., 2016). Collectively these data suggested that ET_AR might indeed

constitute a single drug target that may ameliorate both the renal and inner ear pathologies in Alport syndrome. However, one conundrum to this hypothesis remained in that while pericytes are activated the kidney, previous immunofluorescence studies of whole mount stria vascularis suggested that only marginal and basal cells express ET_AR (Meehan et al., 2016), an observation consistent with earlier reports (Fujimura et al., 1999). Here we show that pericytes cultured from the stria vascularis of young mice do indeed express ET_AR and can be activated in culture by ET-1 to undergo actin cytoskeletal rearrangement.

The RNA-seq data for the stria vascularis from 3-week-old Alport mice relative to wild type littermates suggested activation of cytoskeletal dynamics in one or more of the strial cell types. Dual immunofluorescence studies of whole-mount stria vascularis confirmed that the pericytes show membrane ruffling and detachment with occasional migration into the interstitium of the stria vascularis in these mice. This suggests that the pericytes might be injured by a change in cell signaling caused by the change in the type IV collagen composition of the strial capillary basement membranes previously documented in the Alport mice (Cosgrove et al., 1998). The phenotype is not unlike that recently described for loud noise exposure (Hou et al., 2018). In the case of noise exposure, however, the pericyte detachment and migration was attributed to elevated expression of PDGF-BB. We did not observe induction of PDGF-BB induction in the RNA-seq data, thus it is likely that the detachment/migration phenotype we observed is due to another mechanism; likely ET-1 mediated activation of ET_AR on strial pericytes. It would be of interest to determine whether the 3-week-old Alport mice are more sensitive to noise-induced strial damage than their wild type littermates.

Strial pericytes are an integral part of the intrastrial blood-fluid barrier that is comprised of endothelial cells, the strial capillary basement membranes, the pericytes, and perivascular resident macrophage-like melanocytes (Reviewed in Shi, 2016). They likely play a role in regulating the blood flow through the strial capillaries as they express smooth muscle actin (Nakazawa et al., 1996; Guirdanella et al., 2019) and respond to cytokines by reversibly decreasing the capillary diameter (Bertlich et al., 2017). Following injury by lipopolysaccharide, a biproduct of middle ear infection, pericytes and perivascular macrophages show decreased expression of tight junction proteins and increased expression of MMP-9, which is associated with vascular leakage due to disruption of the blood-fluid barrier (Zhang et al., 2015; Jiang et al., 2019).

The fact that ET-1 stimulates actin cytoskeletal rearrangements in cultured pericytes (Figures 9,10) combined with the observation of pericyte detachment and migration in 3-week-old Alport stria (Figures 5–7) suggests that ET-1 might have something to do with the pericyte detachment and migration, however this possibility remains unexplored. It is compelling that SCBM thickening and progressive accumulation of ECM in the Alport SCBMs can be prevented by treating mice with an ET_AR inhibitor (Meehan et al., 2016). While we show that ET_ARs are expressed on cultured pericytes (Figure 8), ET-1 treatment did not induce expression of ECM, even though laminin α2, α4, and collagen α4(1) are all expressed in these cells (data not shown). It is possible that the strial marginal cells are the source of ECM that accumulates in the SCBMs, since these cells also express ET_ARs (Meehan et al., 2016), and have been previously shown that marginal cells express these ECM molecules

and likely contribute to SCBM homeostasis (Gratton et al., 2002). It remains an open question how or whether pericyte detachment contributes to the pathobiology of progressive dysfunction of the Alport stria vascularis and whether ET_AR blockade would prevent this phenomenon. Overall, this study exemplifies the predictive power of comparative RNA-seq analysis to reveal early events in genetic models for progressive hearing loss.

Supplementary Material

Refer to Web version on PubMed Central for supplementary material.

Acknowledgements

The University of Nebraska DNA Sequencing Core receives partial support from the National Institute for General Medical Science (NIGMS) INBRE - P20GM103427-14 and COBRE - 1P30GM110768-01 grants as well as The Fred & Pamela Buffett Cancer Center Support Grant - P30CA036727. This publication's contents are the sole responsibility of the authors and do not necessarily represent the official views of the NIH or NIGMS. Supported by R01 DC015385 to DC and MAG.

References

Bertlich M, Ihler F, Weiss BG, Freytag S, Strupp M, Canis M 2017 Cochlear pericytes are capable of decreasing capillary diameter in vivo after tumor necrosis factor exposure. Otol. Neurotol 38, e545–e550. [PubMed: 29135875]

Cosgrove D, Meehan DT, Grunkemeyer JA, Kornak JM, Sayers R, Hunter WT Samuelson, G.C. 1996 Collagen 4A3 knockout: A mouse model for autosomal Alport Syndrome. Genes and Development 10, 2981–2992. [PubMed: 8956999]

Cosgrove DE, Samuelson G, Meehan DT, Miller C, McGee J, Walsh EJ & Siegel M 1998 Ultrastructural, physiological, and molecular defects in the inner ear of a gene-knockout mouse model for autosomal Alport syndrome. Hear. Res 121, 84–98. [PubMed: 9682811]

Delimont D, Johnson BM, Meehan DT, Zallocchi M, Gratton MA,Phillips G, Cosgrove D 2014 Laminin 211-mediated FAK activation triggers Alport glomerular pathogenesis. PloS One 9(6):e99083 [PubMed: 24915008]

Drees F, Pokutta S, Yamada S, Nelson WJ, Weis WI 2005 α-catenin is a molecular switch that binds E-cadherin-β-catenin and regulates actin filament assembly. Cell 123, 903–915. [PubMed: 16325583]

Dufek B, Meehan DT, Delimont D, Wilhelm Kevin, Samuelson G, Coenen R, Phillips G, Doyle E, Smyth B, and Gratton MA, Cosgrove D 2019 RNA-seq analysis of gene expression profiles in isolated stria vascularis from wild type and Alport mice reveals key pathways underling Alport strial pathogenesis. Hear. Res In press

Dufek B, Meehan DT, Delimont D, Cheung L, Gratton MA, Phillips G, Song W-P, Liu S, Cosgrove D 2016 Endothelin A receptor activation on mesangial cells initiates Alport glomerular disease. Kidney Int. 90, 300–310. [PubMed: 27165837]

Fujimura T, Furukawa H, Doi Y, Makishima K, Fujimoto S 1999 immunoreactivity of endothelins and endothelin receptor in the stria vascularis of the mouse cochlea. Hear. Res 128, 135–146. [PubMed: 10082294]

Giridharan SS, Rohn JL, Naslavsky N, Caplan S 2012 Differential regulation of actin microfilaments by human MICAL proteins. J. Cell Sci 125, 614–624. [PubMed: 22331357]

Giurdanella G, Montalbano G, Gennusa F, Brancati S, Lo Furno D, Augello A, Buccollo C, Drago F, Salomone S 2019 Isolation, cultivation, and characterization of primary bovine cochlear pericytes: a new in vito model of the stria vascularis. J. Cell Physiol 234, 1978–1986. [PubMed: 30317595]

Gratton MA, Rao V, Meehan DT, Cosgrove D 2002 Strial marginal cells play a role in basement membrane homeostasis: In vitro and in vivo evidence. Hear Res. 163, 27–36. [PubMed: 11788196]

Gratton MA, Rao VH, Cosgrove D 2005 Matrix metalloproteinase dysregulation in the stria vascularis of Alport mice: implications for capillary basement membrane pathology. Am. J. Pathol 166, 1465–74. [PubMed: 15855646]

Hayashi K, Ishikawa R, Ye LH, He XL, Takata K, Kohoma K, Shirao T 1996 Modulatory role of drebrin on the cytoskeleton within dendritic spines in the rat cerebral cortex. J. Neurosci 16, 7161–7170. [PubMed: 8929425]

Hou Z, Wang X, Cai J, Zhang J, Hassan A, Auer M, Shi X 2018 Platelet-Derived Growth Factor Subunit B Signaling Promotes Pericyte Migration in Response to Loud Sound in the Cochlear Stria Vascularis. J Assoc Res Otolaryngol 9, 363–379.

Jiang Y, Zhang J, Rao Y, Chen J, Chen K, Tang Y 2019 Lipopolysaccharide disrupts the cochlear blood-labyrinth barrier by activating perivascular resident macrophages up-regulating MMP-9. Int. J. Pediatr. Otorhinolaryngol 127, 109656. [PubMed: 31470202]

Liu Q, Zou J, Pierce EA 2004 The retinitis pigmentosa 1 protein is a photoreceptor microtubule-associated protein. J. Neurosci 24, 6427–6436. [PubMed: 15269252]

Meehan DT, Delimont D, Cheung L, Zallocchi M, Sansom SC, Holzclaw JD, Rao V, Cosgrove D 2009 Biomechanical strain mediated maladaptive gene regulation as a contributing factor in Alport glomerular disease. Kidney Int. 76, 968–976. [PubMed: 19710627]

Meehan DT, Delimont D, Dufek B, Zallocchi M, Phillips G, Gratton M Cosgrove, D., 2016 Endothelin-1 Mediated Induction of Extracellular Matrix Genes in Strial Marginal Cells Underlies Strial Capillary Basement Membrane Thickening in Alport Mice. Hearing Research, 34, 100–108.

Nakazawa K, Spicer SS, Gratton MA, Schulte BA 1996 Localization of actin in basal cells of the stria vascularis. Hear. Res. 96, 13–19. [PubMed: 8817302]

Neng L, Zhang W, Hassan A, Zemla M, Kachelmeier A, Fridberger A, Aueer M, Shi X 2013 Isolation and culture of endothelial cells, pericytes, and perivascular resident macrophage-like melanocytes from the young mouse ear. Nat. Protoc 8, 709–720. [PubMed: 23493068]

Shi X 2016 Pathphysiology of the cochlear intrastrial fluid-blood barrier (review) Hear,. Res, 338, 52–63. [PubMed: 26802581]

Subramanian A, Tamayo P, Mootha VK, Mukherjee S, Ebert BL, Gillette MA, Paulovich A, Pomeroy SL, Golub TR, Lander ES, and Mesirov JP 2005 Gene set enrichment analysis: a knowledge-based approach for interpreting genome-wide expression profiles. Proc. Nat. Acad. Sci 102, 15545–150. [PubMed: 16199517]

Wu YJ, La Pierre DP, Wu J, Yee AJ, Yang BB 2005 The interaction of versican with its binding partners. 15 483–494.

Zallocchi M, Johnson B, Meehan DT, Delimont D, Rogers KD, Cosgrove D 2013 α1β1 integrin/Rac1-dependent mesangial invasion of glomerular capillaries in Alport syndrome. Am. J. Pathol 183, 1269–1280. [PubMed: 23911822]

Zallocchi M, Johnson B, Meehan DT, Delimont D, Rogers KD, Cosgrove D 2013 α1β1 integrin/Rac1-dependent mesangial invasion of glomerular capillaries in Alport syndrome. Am. J. Pathol 183, 1269–1280. [PubMed: 23911822]

Zhang J, Chen S, Hou Z, Cai J, Dong M, Shi X 2015 Lipopolysaccharide-induced middle ear inflammation disrupts cochlear intra-strial fluid-blood barrier through down regulation of tight junction protiens. PLOS One 10, e0122572. [PubMed: 25815897]

Highlights

1. Strial pathology in the Alport mouse is progressive. At 3 weeks of age hearing loss and SCBM thickening are not evident.
2. RNA-seq analysis of the 3-week-old wild type and Alport stria provide evidence that activation of cytoskeletal dynamics is present in the Alport stria.
3. Whole mount immunostaining confirms activation of cytoskeletal dynamics in strial pericytes.
4. Biochemical and immunohistochemical evidence shows that, like in the renal glomerulus, strial cytoskeletal dynamics in strial pericytes is activated via endothelin-1/endothelin A receptor activation.

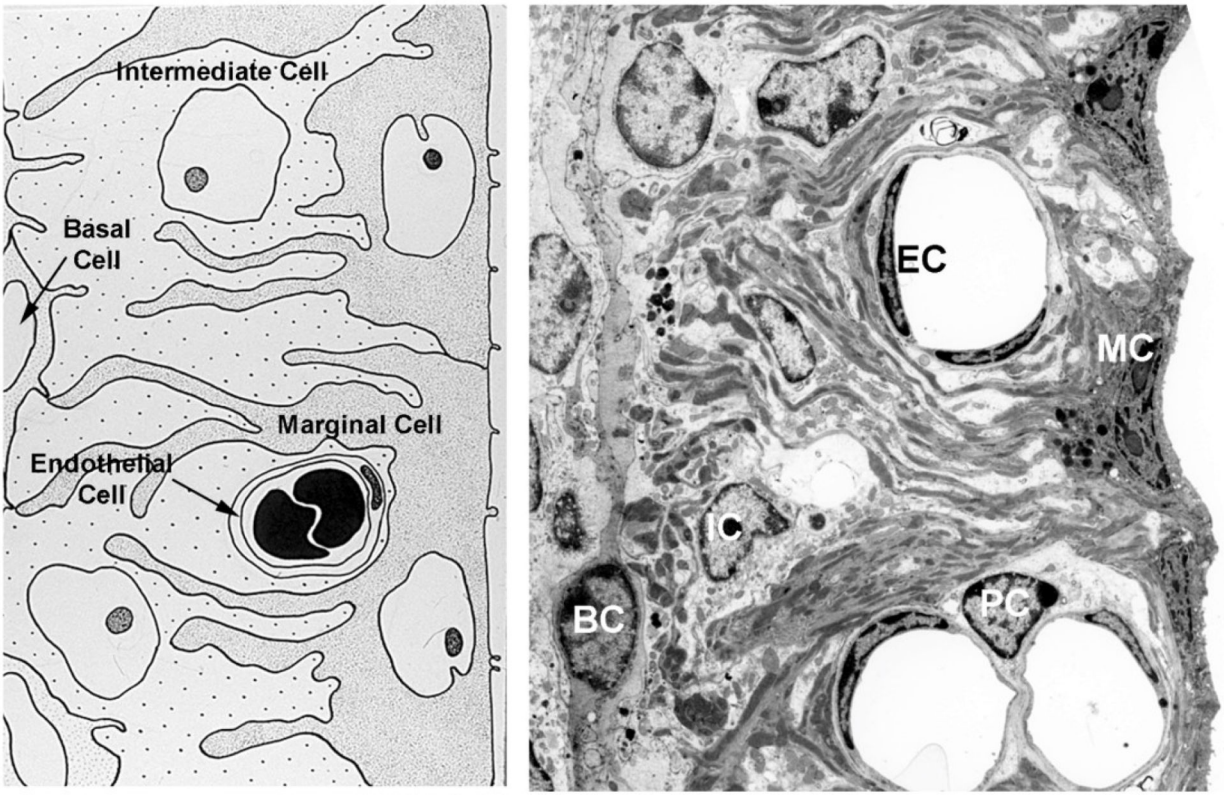

Figure 1.

Cellular architecture of the stria vascularis. The stria consists of luminal marginal cells (MC) that form basolateral infolds with both intermediate cells (IC) and basal cells (BC). The capillaries are consisting of endothelial cells (IC) and pericytes (PC) which are both surrounded by SCBMs.

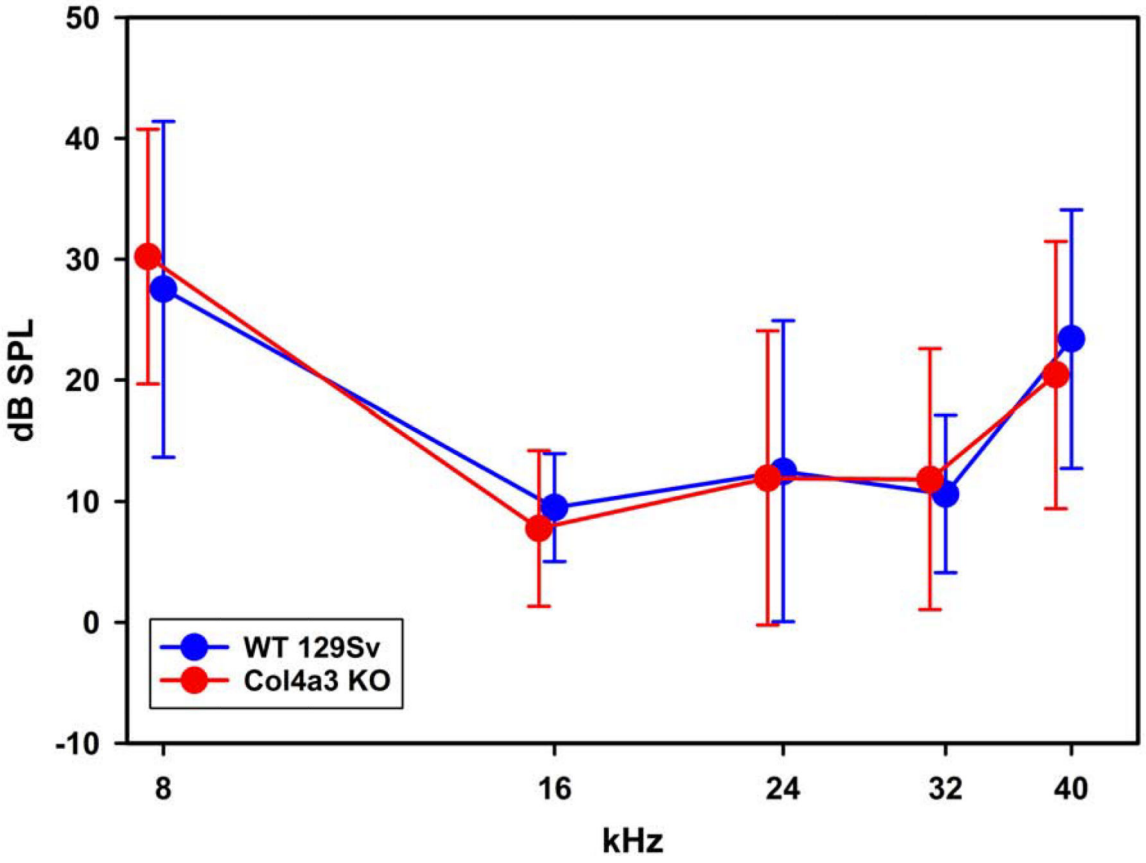

Figure 2.

ABR thresholds indicate that 3-week-old Alport mice have normal hearing. ABR thresholds were determined for 3-week-old wild type and Alport mice. Variances for five individual measurements per cohort are shown. No significant differences were noted for any of the frequencies measured between cohorts (2-Way ANOVA, post-hoc Holm-Sidak).

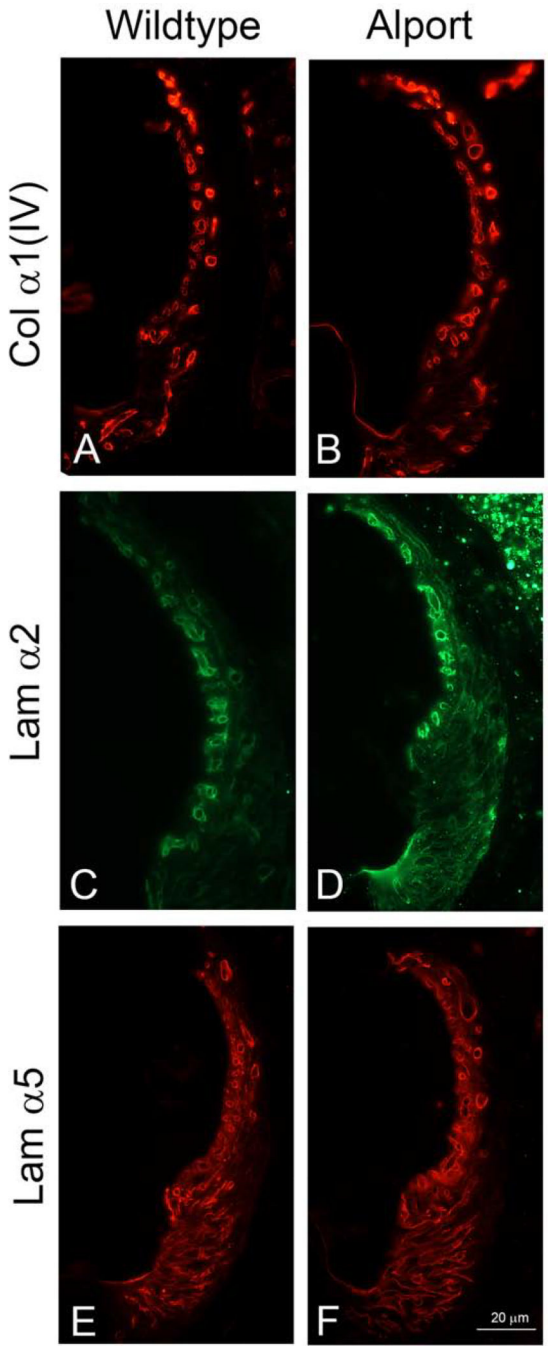

Figure 3.

Immunofluorescence analysis for ECM components in the SCBMs of wild type and Alport stria vascularis show no apparent differences. We previously showed that the SCBM thickening in Alport SCBMs was associated with accumulation of specific extracellular matrix molecules (Gratton et al., 2005; Meehan et al., 2016). This elevated expression is not observed in 3-week Alport mice compared to 3-week wild type mice. Data shown is representative of mid-modiolar sections from 3 animals per cohort. Lamα2 = laminin α2; Lama5 = laminin α5; Collagen IV = the α1 chain of collagen IV.

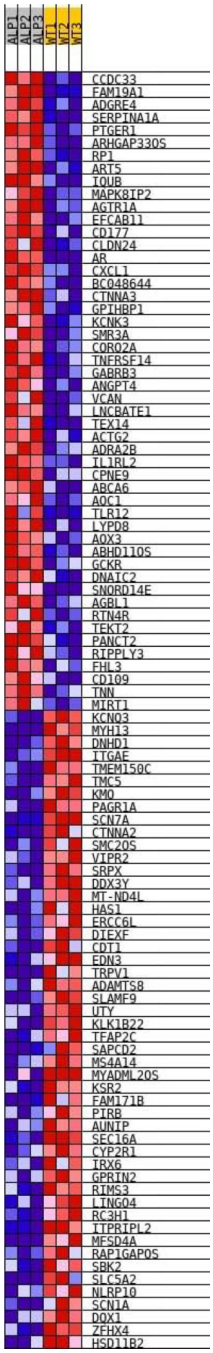

Figure 4.

Heatmap of differentially expressed genes comparing wild type to Alport stria from 3 week old mice. The RNA-seq data was analyzed as described in the methods. The degree of red indicates higher relative expression and blue, lower relative expression across all individual samples analyzed.

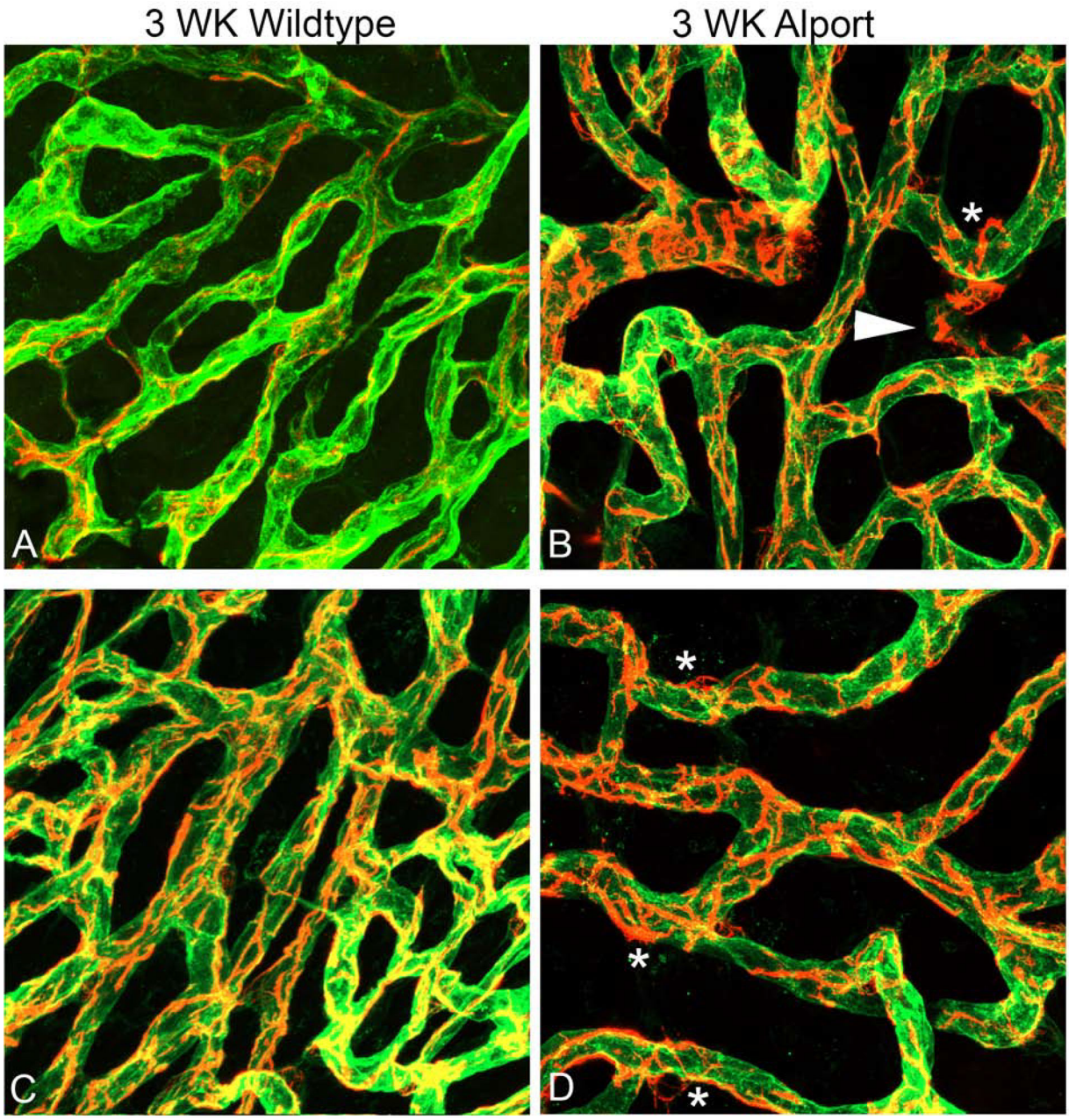

Figure 5.

Dual immunofluorescence immunostaining of whole mount cochlea for Alexa 488-labeled isolectin gs-beta4 and anti-desmin (red) from 3-week-old wild type (A and C) and Alport mice (B and D). Arrowhead: detached pericytes migrating into interstitium. Asterisks: pericytes ruffling. (63X magnification).

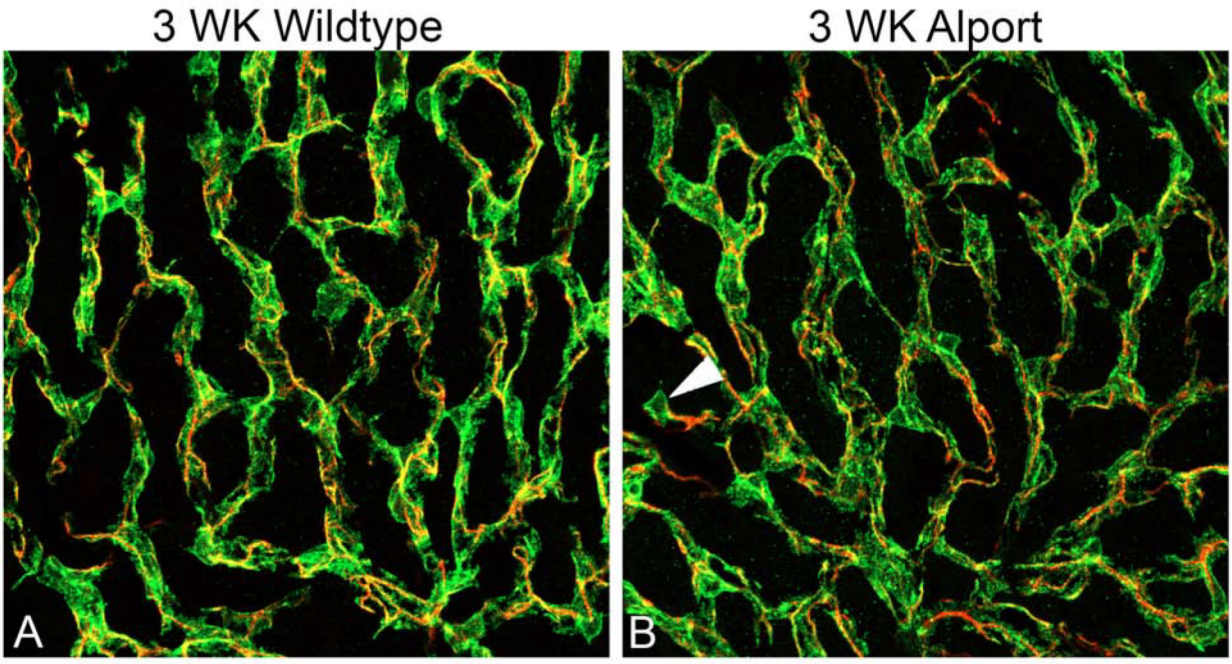

Figure 6.

Dual immunofluorescence immunostaining of whole mount stria with anti-PDGFRb and anti-desmin from 3-week-old wild type (A) and Alport (B) mice. Pericyte somas are labeled with anti PDGFRb antibodies (green); pericyte filaments are labeled with anti-desmin antibodies (red) arrowhead indicates a migrating pericyte in the Alport sample. (40X magnification).

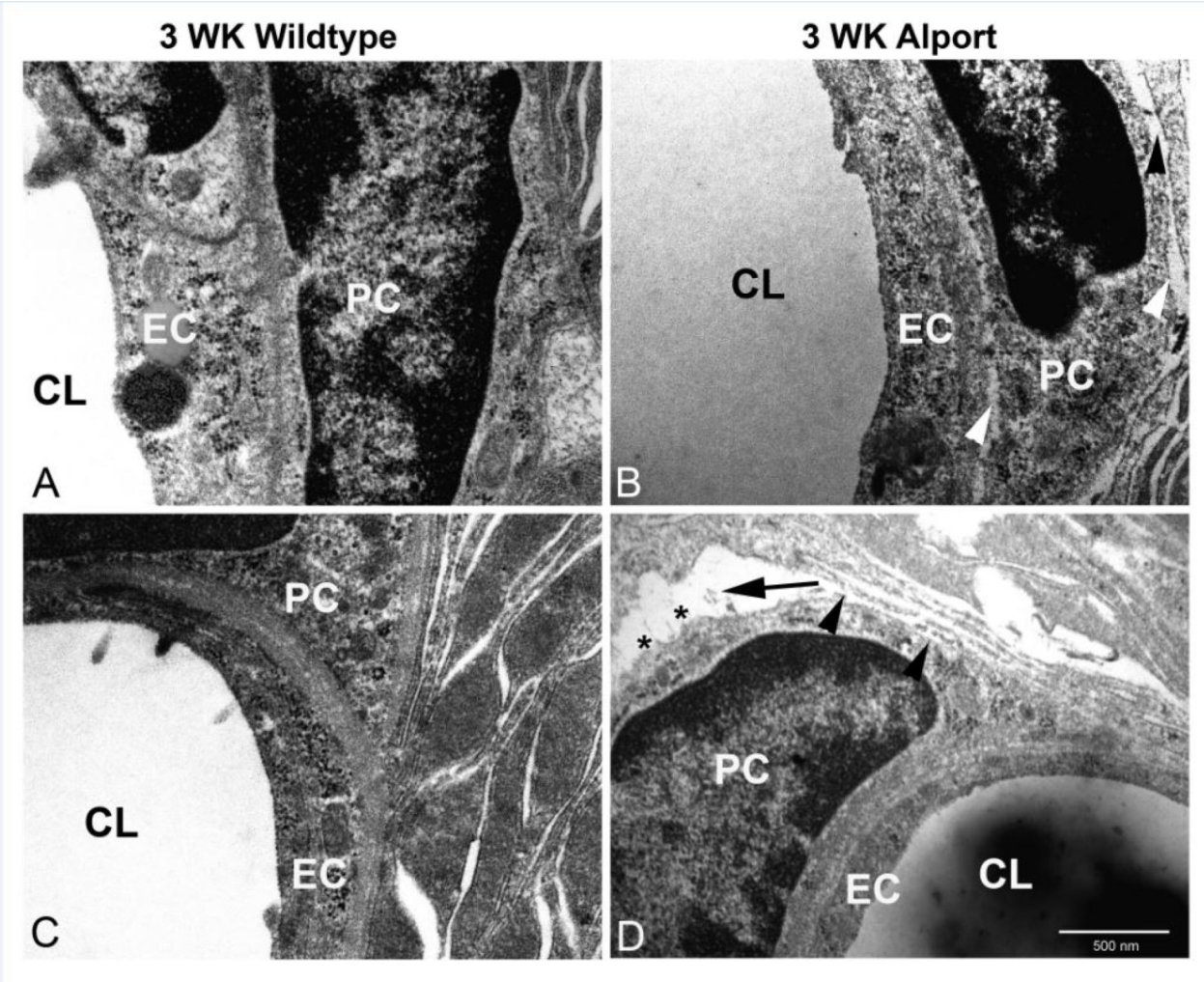

Figure 7.

TEM analysis of pericyte detachment from the SCBMs in 3 week Alport stria. Strial capillaries from wild type mice show tight adherence between the pericytes and the epithelial/endothelial basement membranes (panels A and C). Alport strial capillaries occasionally show detachment Panels B and D, arrowheads) and less occasionally severe detachment (panel D arrow) with apparent membrane ruffling (panel D asterisks). These anomalies were never observed in the wild type strial capillaries. CL: capillary lumen; EC: endothelial cell; PC: pericyte.

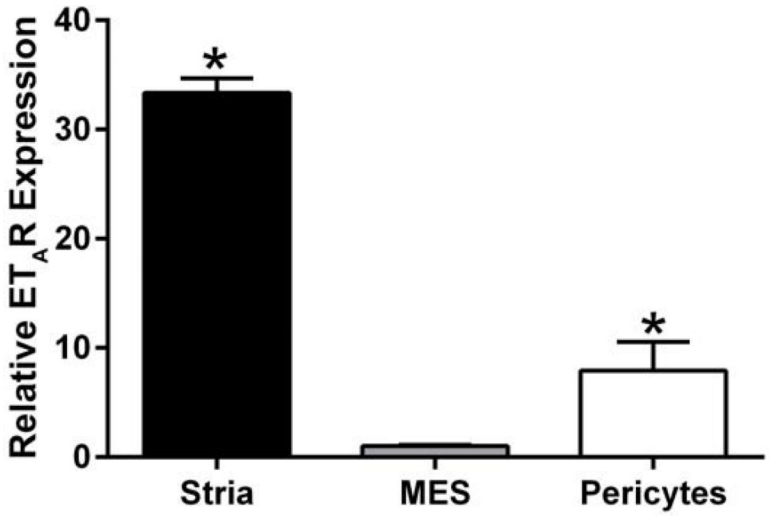

Figure 8.

Endothelin A receptors are expressed in both the stria vascularis and in cultured pericytes. RNA from the stria vascularis from wild type mice, cultured primary mesangial cells (positive control), and cultured primary pericytes were examined using real time RT-PCR. The experiment was performed in triplicate and analyzed by two-tailed student's t-test. Asterisks denote significant differences ($p<0.05$) when compared to mesangial cell RNA (MES).

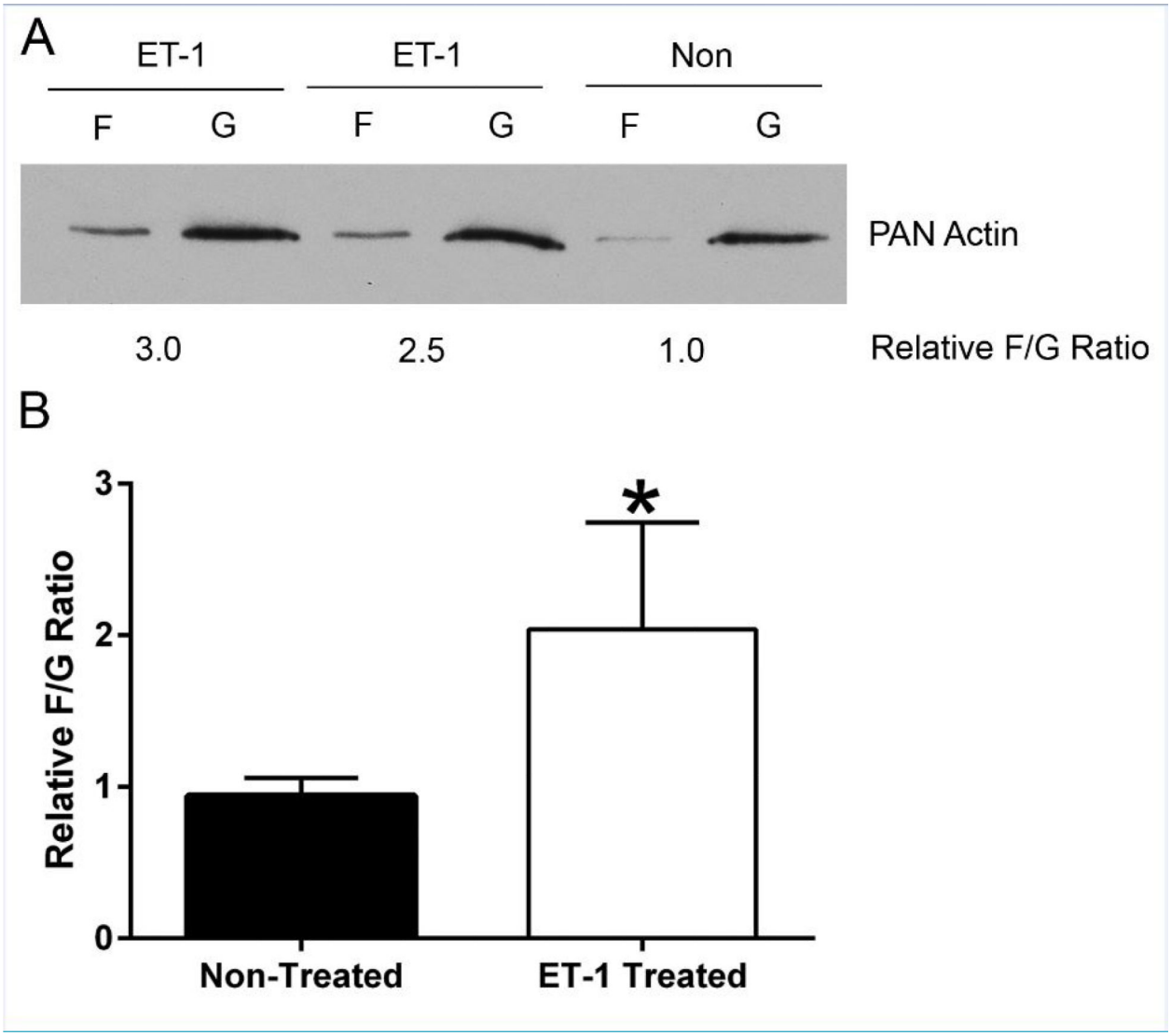

Figure 9.

ET-1 effects on Actin Polymerization (F/G ratios) in Pericyte Cell Culture. Equal amounts of Pericytes cell lysates were subjected to differential centrifugation to separate filamentous actin (F-actin) from globular actin (G-actin) and Pan Actin immunoblots were performed from each sample (A). The corresponding bands were quantified and expressed as the F-actin/G-actin ratio. An increase of actin polymerization (F/G ratio) by ET-1 treatment was observed. This was quantified by densitometry for four independent experiments (B) using one-sample t test (hypothetical mean=1) * denotes a significant difference in F/G ratio for Et-1-treated versus non-treated cells.

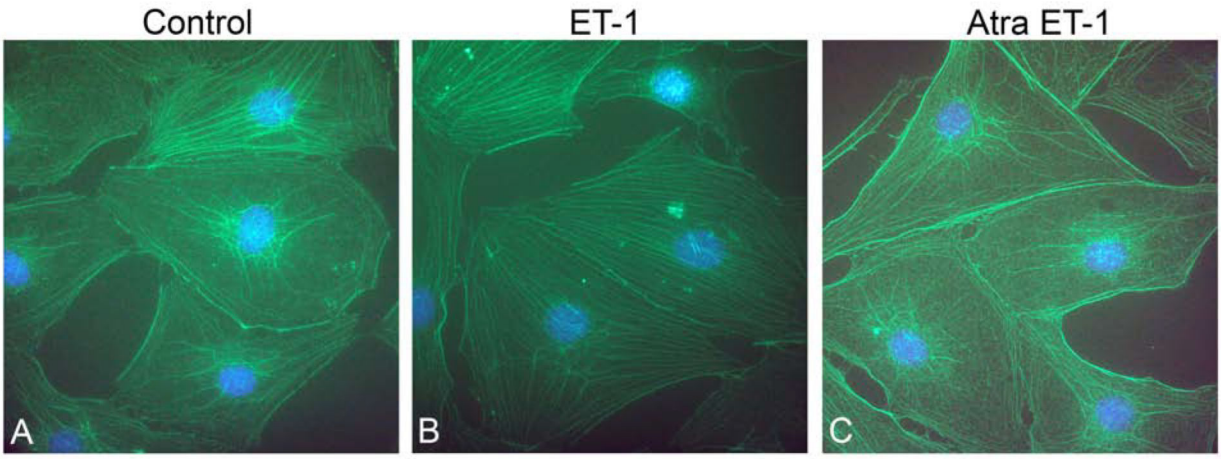

Figure 10.

ET-1 treatment of cultured pericytes results in an increase in actin filaments. Cells were treated vehicle (panel A), with ET-1 for 1 hour (panel B), or with a combination of ET-1 and the ETAR antagonist Atrasentan (panel C), and then fixed with acetone. Dual staining was performed using phalloidin (green) and anti-drebrin antibodies (red). Nuclei were stained with DAPI.

Table 1.

RNA-seq analysis of 3-week WT versus Alport stria vascularis.

Cell-To-Cell Signaling and Interaction: Adhesion of tumor cell lines			
		Fold Change Alp vs WT	
Gene Name	**Protein**	**Average**	**Std Dev**
Vcan	versican	11.75	5.83
Ctnna3	catenin (cadherin associated protein), alpha 3	4.30	0.87
Apoh	apolipoprotein H	2.24	0.15
Cdcp1	CUB domain containing protein 1	1.69	0.10
Itgal	integrin alpha L	1.65	0.26
Cell Death and Survival: Regeneration of axons			
		Fold Change Alp vs WT	
Gene Name	**Protein**	**Average**	**Std Dev**
Rtn4r	reticulon 4 receptor	1.87	0.44
Cell Morphology: Formation of cellular protrusions			
		Fold Change Alp vs WT	
Gene Name	**Protein**	**Average**	**Std Dev**
Tex14	testis expressed gene 14	14.50	8.05
Mapk8ip2	mitogen-activated protein kinase 8 interacting protein 2	3.40	0.92
Tnn	tenascin N	3.33	0.58
Gabrb3	gamma-aminobutyric acid (GABA) A receptor, subunit β3	2.02	0.16
Lrrc4	leucine rich repeat containing 4	1.93	0.30
Rtn4r	reticulon 4 receptor	1.87	0.44
Ctnna2	catenin (cadherin associated protein), alpha 2	−2.44	.24
Ksr2	kinase suppressor of ras 2	−4.35	5.29
Cell Morphology: Sprouting			
		Fold Change Alp vs WT	
Gene Name	**Protein**	**Average**	**Std Dev**
Tnn	tenascin N	3.33	0.58
Gabrb3	gamma-aminobutyric acid (GABA) A receptor, subunit β3	2.02	0.16
Lrrc4	leucine rich repeat containing 4	1.93	0.30
Ctnna2	catenin (cadherin associated protein), alpha 2	−2.44	0.24
Cell Signaling: Small GTPase mediated signal transduction/Rho Protein signal transduction			
		Fold Change Alp vs WT	
Gene Name	**Protein**	**Average**	**Std Dev**
Agtr1a	angiotensin II receptor, type 1a	3.08	0.62
Rtn4r	reticulon 4 receptor	1.87	0.44
Lpar2	lysophosphatidic acid receptor 2	1.75	0.24
Cellular Assembly and Organization: Depolymerization of filaments			
		Fold Change Alp vs WT	
Gene Name	**Protein**	**Average**	**Std Dev**
Rp1	retinitis pigmentosa 1 (human)	2.53	0.50

Mical2	microtubule associated monooxygenase, calponin and LIM domain containing 2	−1.54	0.07

Cellular Assembly and Organization: Formation of cytoskeleton

		Fold Change Alp vs WT	
Gene Name	**Protein**	**Average**	**Std Dev**
Rp1	retinitis pigmentosa 1 (human)	2.53	0.50
Ar	androgen receptor	2.11	0.19
Lpar2	lysophosphatidic acid receptor 2	1.75	0.24

Cellular Assembly and Organization: Formation and Polymerization of microtubules

		Fold Change Alp vs WT	
Gene Name	**Protein**	**Average**	**Std Dev**
Rp1	retinitis pigmentosa 1 (human)	**2.53**	**0.50**

Cellular Assembly and Organization: Organization of cytoskeleton

		Fold Change vs. WT	
Gene Name	**Protein**	**Average**	**Std Dev**
Tex14	testis expressed gene 14	14.50	8.05
Fhl3	four and a half LIM domains 3	3.62	0.87
Mapk8ip2	mitogen-activated protein kinase 8 interacting protein 2	3.40	0.92
Tnn	tenascin N	3.33	0.58
Rp1	retinitis pigmentosa 1 (human)	2.53	0.50
Ar	androgen receptor	2.11	0.19
Gabrb3	gamma-aminobutyric acid (GABA) A receptor, subunit β3	2.02	0.16
Lrrc4	leucine rich repeat containing 4	1.93	0.30
Rtn4r	reticulon 4 receptor	1.87	0.44
Mical2	microtubule associated monooxygenase, calponin and LIM domain containing 2	−1.54	0.07
Aunip	aurora kinase A and ninein interacting protein	−1.92	0.59
Ctnna2	catenin (cadherin associated protein), alpha 2	−2.44	0.24
Ksr2	kinase suppressor of ras 2	−4.35	5.29